Anomalies in vortex lattice dynamics driven by induced ac currents in superconducting films with magnetic arrays of two-fold symmetry

2015 Supercond. Sci. Technol. 28 015001

(http://iopscience.iop.org/0953-2048/28/1/015001)

IOP Publishing Superconductor Science and Technology
Supercond. Sci. Technol. **28** (2015) 015001 (8pp) doi:10.1088/0953-2048/28/1/015001

Anomalies in vortex lattice dynamics driven by induced ac currents in superconducting films with magnetic arrays of two-fold symmetry

A J Moreno[1,5], C E Chiliotte[1], G Pasquini[1], V Bekeris[1], A Gomez[2], J del Valle[2], E M Gonzalez[2,3], J L Prieto[4] and J L Vicent[2,3]

[1] Departamento de Física, Facultad de Ciencias Exactas y Naturales, Universidad de Buenos Aires, Buenos Aires 1428, and IFIBA CONICET, Argentina
[2] Departamento de Física de Materiales, Facultad de CC. Físicas, Universidad Complutense, E-28040 Madrid, Spain
[3] IMDEA-Nanociencia, Cantoblanco, E-28049 Madrid, Spain
[4] ISOM-ETSIT, Universidad Politécnica de Madrid, E-28040 Madrid, Spain

E-mail: vbekeris@df.uba.ar

Received 16 July 2014, revised 1 October 2014
Accepted for publication 14 October 2014
Published 26 November 2014

Abstract

We study the dynamics of the vortex lattice driven by ac induced currents in the critical state regime, for $T > 0.70\ T_C$. The samples are superconducting films grown on top of two-fold symmetry array of magnetic dots. In these heterostructures, the induced ac currents flow parallel to the short and to the long side of the pinning array in different areas of the samples simultaneously. This behavior produces remarkable effects in the vortex lattice dynamics. First of all, periodic features are observed in the ac susceptibility versus applied magnetic field measurements which are related to matching effects between the vortex lattices and the magnetic array. However, the vortex lattice reconfiguration observed in magnetotransport experiments is absent. Some of these features are revealed as maxima instead of being minima, indicating higher mobility at certain matching fields. Competing unstable vortex configurations could lead to increase vortex mobility precluding the reconfiguration transition. At high temperatures, where the matching effects show up, the magnetic permeability of the dots is the mechanism that governs the $J_C(T)$ behavior. Moreover, the temperature dependence of the pinning force $F_P(T)$ shows a temperature crossover related to an unexpected enhancement in vortex mobility. Vortex–vortex interaction and the interplay between trapped and interstitial vortices are a hint to explain these phenomena.

Keywords: superconducting film, vortex lattice, two-fold magnetic array, ac induced currents

(Some figures may appear in colour only in the online journal)

1. Introduction

Periodic arrays of submicrometric magnetic dots efficiently stabilize the vortex lattice (VL) in superconducting films [1], with the symmetry of the underlying array structure. In films containing high symmetry triangular [2, 3], square [4, 5] or Kagome arrays [6] of magnetic dots, the resistivity versus magnetic field presents minima at regular field intervals that correspond to the VL matching the array of dots [2]. Additionally, the critical current density shows periodic maxima at the same regular field intervals [4, 7]. These effects may depend on the current orientation and temperature [8].

[5] We regret to inform that A J Moreno passed away in January 2014.

On the other hand, for low symmetry pinning landscapes, the driven VL presents interesting peculiarities. In the case of a classical low temperature superconductor [9, 10] containing a two-fold symmetry rectangular array of magnetic dots, the low field VL adopts the rectangular configuration of the pinning array, and transport properties for currents parallel to the long side of the rectangle show periodic magnetoresistance minima and critical current maxima at field intervals matching the rectangular cell of the pinning landscape. As field is increased, the vortex lattice becomes stiffer and elastic energy increases above the pinning energy, giving rise to a reconfiguration transition from a rectangular to a square vortex lattice, revealed by the periodic response at a higher field interval that corresponds to a square unit cell with sides very close to the short side of the rectangular array.

Transport experiments can be realized only within a small temperature interval close to the sample critical temperature [1], typically $T > 0.97\ T_C$, and consequently using magnetotransport experiments a broad temperature window remains unexplored. At lower temperatures, elastic and pinning energies both increase, and different pinning mechanisms, as intrinsic random pinning, may eventually compete with periodic pinning. Therefore, the examination of these systems at lower temperatures needs to be addressed and calls for alternative methods.

In a previous work [11], we have used ac susceptibility techniques, χ_{ac}, to study the dynamics of the VL in a wide temperature range below T_C, and we found that in samples containing a square array of Ni dots matching effects far from T_C preserve the general behavior found with the use of transport techniques in similar samples. In contrast, for samples containing the two-fold rectangular pinning array, although matching periodicity in $\chi_{ac}(H)$ corresponds to the rectangular primitive cell, some of the matching orders were surprisingly missing and even some of them showed increased mobility in contrast to the expected increased pinning. Moreover, our $\chi_{ac}(H)$ results showed no signs of a reconfiguration transition.

In this paper we investigate these striking features and their physical origin by means of ac susceptibility experiments in Nb film containing a rectangular array of Ni dots. The temperature dependence of the pinning forces was determined and compared with theoretical models for pinning potentials based on different mechanisms [4]. Critical current density, $J_C(T)$, was calculated following a known procedure [12], first identifying the range of ac amplitude and temperature where the sample is in Bean critical state (CS) regime [13]. In this framework, in the field penetrated region of the sample, the induced current density is uniform. This current is determined by the balance between Lorentz and pinning forces, and we assume the azimuthal currents are isotropic.

By comparing the temperature dependence of the experimental pinning forces at the matching fields with theoretical models [4] we were able to identify the prevailing pinning interactions. The pinning force per volume $F_P(T, H)$ shows, above a field dependent crossover temperature, the behavior predicted for vortex pinning by the high permeability of ferromagnetic dots [3–5, 14]. As field is increased the lattice becomes stiffer and we find that this regime extends to lower temperatures. Interestingly, we find that in this regime, at the second matching field, the extra interstitial vortex line does not contribute significantly to pinning. As temperature is reduced, intrinsic pinning comes gradually into play [4].

We also find an anomalous increase in mobility at the third matching field, for which a rectangular and a square VL arrangement probably compete.

The paper is organized as follows: in the next section we describe the experimental details, in section 3 we present results and discussions and a summary and conclusions are drawn in section 4.

2. Experimental

The sample consists of a Nb film $0.9 \times 3\ mm^2$ of thickness 100 nm containing a rectangular array of Ni dots, with diameter $D = 200$ nm and thickness $\varepsilon = 40$ nm. The array cell has an aspect ratio $a_R = c/b = 600\ nm/400\ nm = 3/2$, and is parallel to the sample edges. It was fabricated on Si (100) substrates using electron beam lithography and lift-off technique in combination with dc magnetron sputtering [15]. The physical size of the dot array is equal to the sample size. The e-beam lithography was performed with a CRESTEC CABL-9000C. This system is specially designed to have high beam stability, both in current and position. The lithography room temperature is controlled and therefore, the thermal controller of the machine works in optimized conditions and the usual beam current stability is $< 0.2\%$ in 10 h. The same applies for the beam position stability and the stitching accuracy. These characteristics combined allow extremely precise long exposures of dots or other features, and the boundaries between the 60 μm fields are virtually impossible to find.

The first calculated matching field is $H_1{}^R = \phi_0/(b\ c) = 86$ Oe, where $\phi_0 = 2 \times 10^{-7}\ G\ cm^2$ is the flux quantum, while the matching field for a reconfigured square VL with sides equal to the short side b of the rectangular pinning cell is $H_1{}^S = \phi_0/b^2 = 129$ Oe. Note that for the dimensions of the square of side b and the rectangle of sides $b \times c$, there is coincidence in matching for applied magnetic fields $H_k = 3\ k\ H_1{}^R = 2\ k\ H_1{}^S$, where k is an integer. We will come back to this point below.

The measurements were performed in a Quantum Design MPMS superconducting quantum interference device (SQUID) magnetometer, for both ac and dc magnetic fields applied perpendicular to the sample surface. Complex ac susceptibility, $\chi_{ac} = \chi'(H, T) + i\,\chi''(H, T)$ [16], is related to the currents, $j(t)$, induced by the applied ac field $h(t) = h \cos(\omega t)$ superimposed to the dc field, H. The resulting time dependent magnetization, $M(t)$, of the sample is then periodic in $2\pi/\omega$ and is given by

$M(t) = \frac{1}{2cV} \int_V \bar{r} \times \bar{j}(t)\ dV$ where V is the sample volume. The first Fourier components of $M(t)$ are χ' and χ''. The ac susceptibility real component, χ', is in direct relation to the penetration of ac field in the sample. The out of phase

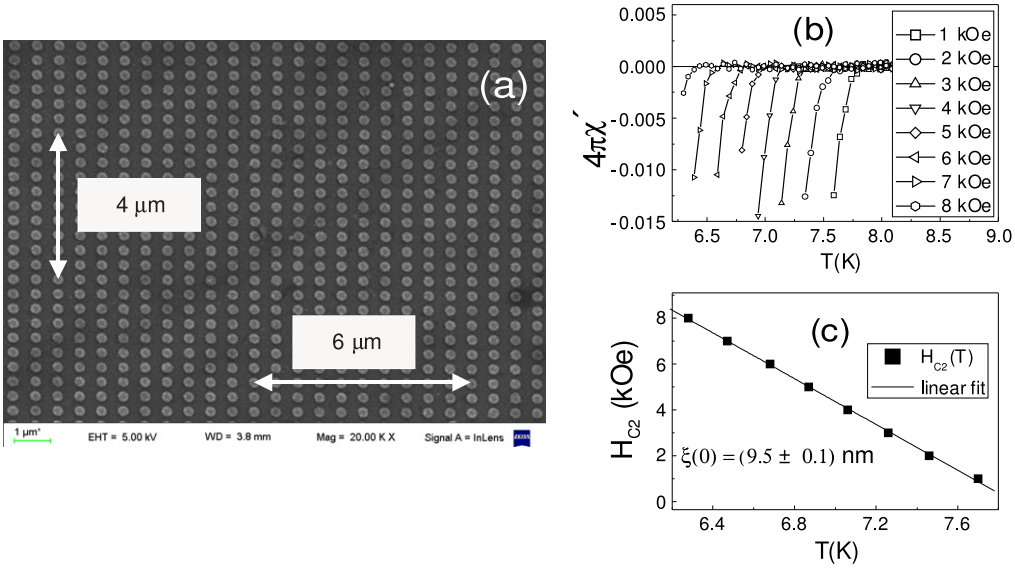

Figure 1. (a) SEM micrograph (×20 000) of the Nb film containing a rectangular array of Ni nanodots. Labels indicate dimensions for ten consecutive cells. (b) $4\pi\chi'$ (T) for different applied dc fields, between 1 and 8 kOe in FC experiments, showing the field dependent onset of the superconducting transition. (c) H_{C2} (T) boundary in symbols. The line is a fit (see text) with $\xi_{GL}(0)$ the zero temperature coherence length as the only fitting parameter.

component, χ'', measures the dissipation due to the electric field induced by changes in the magnetic flux in the sample.

Small ac penetration depth or high screening ($\chi'(H, T) \sim -1/4\pi$), is related to a highly pinned VL with low mobility. Losses on the other hand, tend to zero for highly screened ac fields (*e.g.* at low temperatures) that produce no changes in the magnetic flux in the sample. Oppositely, a large ac penetration depth in a weakly pinned, highly mobile VL leads to full penetration and negligible $M(t)$, thus both χ' (H, T) and χ'' (H, T) ~ 0. As a result, χ'' is a non monotonic function and displays a peak as a function of temperature (see figure 3(a)). For ac fields that force vortices to perform excursions outside the effective pinning wells, χ_{ac} (H, T) is dependent on the applied ac field amplitude and losses are not negligible.

To identify the CS regime [13], the ac field amplitude, h, was varied between 0.25 and 2 Oe in $\chi_{ac}(T)$ experiments at frequency $f = 1$ kHz to cover a wide range of induced current densities, as will be described below. On the other hand, synchronized pinning in CS was examined in isothermal $\chi_{ac}(H)$ measurements, for $h = 1$ Oe in zero field cooled samples. Temperature was controlled better than 1 mK during field variation. The critical temperature at zero field, $T_C = 7.95$ K, was determined for $h = 0.1$ Oe and the 10% to 90% transition width was ~0.55 K.

3. Results and discussion

Figure 1(a) shows a scanning electron microscopy (SEM) image of the sample (magnification 20 000) containing the periodic array of Ni dots of dimensions described above, and labels show the dimensions for ten cells.

It is known that each dot in the array may accommodate more than one vortex, either as a single multiquanta vortex or in the form of multiple confined vortices [17]. A rough estimation of the occupation number S_N can be obtained for a pattern of periodic pinning sites by $S_N = D/4\xi$ [17], D and ξ being the dot diameter and the coherence length, respectively. Therefore, to evaluate the occupation number we need to estimate ξ (T). These values are extracted, as usual, from the upper critical field $H_{C2}(T)$ data.

In figure 1(b) we show χ' (T) for various dc fields. The field was applied in the normal state before cooling the sample. The resulting $H_{C2}(T)$ is plotted in panel (c) and fitted to the expression $H_{C2}(T) = \phi_0/[2\pi \xi^2_{GL}(T)]$ with $\xi_{GL}(T) = \xi_{GL}(0)\ (1 - T/T_C)^{-1/2}$ the Ginzburg–Landau coherence length, resulting $\xi_{GL}(0) = (9.5 \pm 0.1)$ nm being the only fitting parameter.

Before we present our isothermal $\chi'(H)$ results, we briefly summarize some of the observations in transport experiments reported elsewhere [9.10] for samples containing a rectangular array of Ni dots, similar to the ones studied in the present paper.

Magnetoresistance experiments in Nb films with a rectangular array of submicrometric Ni dots reveal two different pinning regimes of the VL [1, 2, 10] with both regimes showing periodic resistivity minima as function of applied field. At low applied fields, the interval between minima coincides with the matching field for the rectangular pinning array leading to the conclusion that pinning energy dominates at large intervortex distances and the VL acquires two-fold symmetry. This generalized observation for films containing rectangular arrays of artificial pinning centers has been theoretically studied [19].

For increasing magnetic field, elastic energy of the vortex lattice increases over the pinning energy, and above a weak

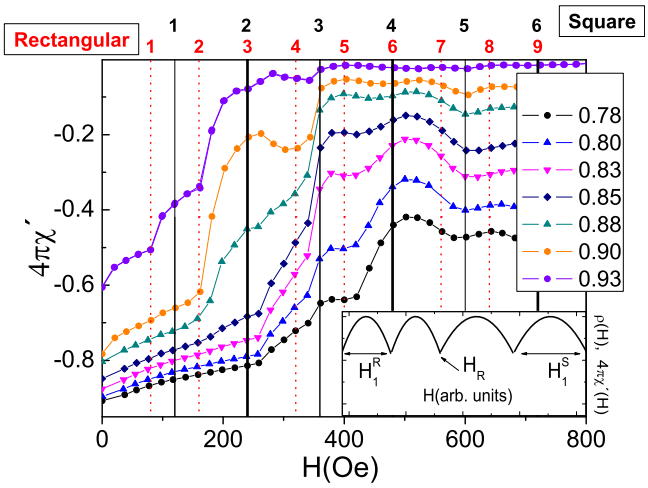

Figure 2. Ac susceptibility ($h = 1$ Oe, $f = 1$ kHz) versus applied dc field at different reduced temperatures. Dotted red vertical lines indicate matching fields for the rectangular pinning array $H = n^R H_1{}^R$, n^R is indicated in red in the lower line at the top of the figure. Full black vertical lines indicate matching fields for the short side square symmetry of the array, $n^S H_1{}^S$ and n^S is indicated in black in the upper line at the top of the figure. Thick black vertical lines show coinciding matching for both arrays, $3\text{ k } H_1{}^R = 2\text{ k } H_1{}^S$ for $k = 1$, 2 and 3. Inset: scheme of the expected periodic dips in resistivity, $\rho(H)$ and in $\chi'(H)$ for a rectangular VL at low fields with periodicity $H_1{}^R$ and a reconfigured square VL at higher fields with periodicity $H_1{}^R$, assuming multiple vortex occupation.

temperature dependent 'reconfiguration' field $H_R(T)$, the VL modifies its configuration to relax its elastic energy. The new field interval between successive resistivity minima for fields larger than $H_R(T)$ is close to the matching field of a square vortex lattice, of sides equal to the short side of the pinning array unit cell [9]. In these transport experiments the current was applied parallel to the long side of the rectangle, and the Lorentz force drove the vortex lattice along the short side of the dot array, pinning more efficiently the VL when it matched the short side of the pinning array. The inset in figure 2 shows schematically the periodic dips in resistivity $\rho(H)$ at matching conditions (periodic increase in pinning) that should be qualitatively similar to $\chi'(H)$ response. For a VL that conserves a rectangular symmetry, the field periodicity is $H_1{}^R$ and as field is increased the lattice reconfigures to a square VL of sides equal to the shorter side of the rectangle, and the periodicity increases to $H_1{}^S > H_1{}^R$. The reconfiguration field H_R is indicated. In this scheme, multiple vortex occupation is assumed, so that the dips and maxima are independent of magnetic field. However, if additional vortices that penetrate with increasing field occupy interstitial positions, minima and maxima in resistivity or in susceptibility should increase with field.

The intensity of the driving current certainly plays an important role in vortex dynamics and the resistivity minima are present in field dependent current range [4, 20].

We now turn to our $\chi'(H)$ data. The sample was cooled from above T_C to the target temperature in zero field (ZFC). Figure 2 shows the real part of ac susceptibility as a function of dc field at temperatures between 0.78 T_C and 0.93 T_C, for $h = 1$ Oe. In the experimental temperature window from T_C to the lowest value $T = 0.7$ T_C the occupation number S_N is between 1 and 2 vortices per dot. However, if dots pin multiquanta, $\chi'(H)$ should in average be almost constant [10] (see inset in figure 2) and the dips or cusps in $\chi_{ac}(H)$ should be independent of H. In contrast, our results in figure 2 show strong field dependence, suggesting that only one flux quantum is strongly pinned to each Ni dot when the VL exactly matches the artificial pinning array, and the excess vortices as field is increased are forced into interstitial positions where vortices become more mobile and ac penetration increases [10]. Additionally, we find that the obtained $\xi_{GL}(0)$ leads to a coherence length $\xi_{GL}(T)$ smaller than the width of the superconducting stripes between dots, $W = 200$ nm, consistent with the observed linear dependence of $H_{C2}(T)$ in figure 1(c). So, the possible scenario of superconducting wire network [18] is ruled out, we are dealing with pinning mechanisms only.

We find that field periodicity is not as regular as in transport experiments in similar samples [9, 10], and we examine in the following the possible mechanisms that lead to this unexpected response.

Vertical lines indicate the different calculated matching fields: (i) in dotted lines for multiples of the first matching field, $H_1{}^R$, for a rectangular array, (ii) in full lines for multiples of the first matching field, $H_1{}^S$, for a square array of sides equal to the short side of the rectangle, and we label, at the top of the figure, the matching order for the square VL cell in the upper line and for the rectangular cell in the lower line. On the other hand, thick lines indicate the coincidence of different multiples n^R and n^S of $H_1{}^R$ and $H_1{}^S$ respectively. Local minima [11] in χ' for some of the multiples of $H_1{}^R$, indicate that VL synchronization with the rectangular array extends to high matching orders although some intermediate orders are absent. Surprisingly, there is no enhancement of pinning with the square field periodicity $H_1{}^S$, expected above the reconfiguration transition from rectangular to square symmetry that takes place when elastic energy dominates over pinning energy.

At the lowest examined temperatures, matching is blurred for low fields and this is understood as arising from the increase in random intrinsic pinning at low temperature. For $H_1{}^R$ we find no matching effects for $T \leqslant 0.90$ T_C and for $2H_1{}^R$ no matching occurs for $T \leqslant 0.83$ T_C. This result helps to discriminate between the different possible pinning mechanisms at low temperature, because lack of matching effects implies the contribution of random intrinsic pinning, as will be described below.

Moreover, mobility increases for matching fields that, due to the aspect ratio of the array, coincide with both rectangular and square VL configurations, for $n^R = 3$ and $n^S = 2$ for reduced temperature $t = T/T_C > 0.88$ in figure 2, and for $n^R = 6$ and $n^S = 4$ in the whole T range.

These results suggest a competition between rectangular and square VL periodicity for the first matching coincidence, $n^R H_1{}^R = 3\text{ k } H_1{}^R = n^S H_1{}^S = 2\text{ k } H_1{}^S$ ($n^R = 3$ and $n^S = 2$) where

$k = 1, 2, 3\ldots$ at high temperature, and for the whole examined temperature range at higher fields ($n^R = 6$ and $n^S = 4$). The system does not find a preferred configuration and is therefore not efficiently pinned, showing higher vortex mobility. This effect may be probably promoted by the driving current flow that is oriented in nearly perpendicular directions in different regions of the sample, forcing vortices to move in directions parallel or perpendicular to the long side of the rectangular pinning array, in different regions of the sample.

In relation to the current orientation, the changeover from a rectangular to square VL has been observed in magnetoresistance experiments for Lorentz forces with different orientations [8], so the resistivity minima occur when the square VL matches the dot array along the direction of vortex motion, or for vortex velocities locked in direction of the small side of the pinning array. Up to a given VL velocity threshold the motion in rectangular pinning arrays is guided along the short side of the array [8]. In contrast, ac susceptibility experiments induce azimuthal ac currents that flow parallel to the short and to the long side of the pinning array in different regions of the sample simultaneously. Therefore, this competition could prevent the reconfiguration of the VL from rectangular to square when the applied magnetic field increases.

In addition, the magnitude of the induced currents may also contribute to the observed phenomenology [8, 20]. However, it has been shown elsewhere in ac susceptibility experiments [11] that for a square pinning array, where induced currents are close to J_C as well, regular fractional and integer matching effects in $\chi_{ac}(H)$ are displayed, discarding that the magnitude of the ac driving currents is the only origin of the observed irregular periodicity in samples with two-fold symmetry pinning arrays.

3.1. The critical state and $J_C(T,H)$ calculation

To clarify the origin of the irregular field periodicity in VL dynamics, we address below the nature of pinning mechanisms. Different vortex pinning mechanisms by Ni dots have been proposed either originated in magnetic interactions between vortex lines and Ni dots or as a result of local suppressed superconductivity close to the dot by magnetic proximity effect or dot stray field.

Consequently, there are several magnetic mechanisms to consider: (i) the interaction of vortex lines with normal regions around the dots caused by the dot stray field or the ferromagnetic proximity effect, (ii) the interaction between the vortex magnetic field and the magnetic dipole of the dot or (iii) interaction of vortex lines with dots due to the higher permeability at the dot. Martin and coworkers (see [4]) discuss these mechanisms in detail, and they show that the temperature dependence of the pinning force between a vortex line and a pinning center, $F_P(T)$, directly associated with the critical current density, $J_C(T)$, can be fitted to an expression proportional to $(1 - T/T_C)^N$, where N identifies the pinning mechanism. Their prediction was made close to T_C, but we show below that their results can be extended satisfactorily to our lower temperature range.

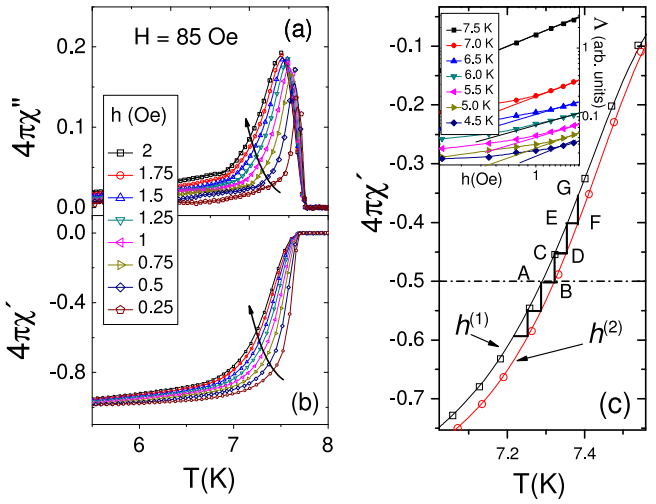

Figure 3. (a) $\chi''(T)$ and (b) $\chi'(T)$ for $h = 0.25$ to 2 Oe, $f = 1$ kHz and applied field $H = 85$ Oe. Arrows indicate increasing ac amplitude. (c) Main panel shows $\chi'(T)$ for two ac amplitudes, $h^{(1)} = 2$ Oe and $h^{(2)} = 1.75$ Oe and a sketch of the method to determine $\Lambda(\chi'(h))$ described in the text. The dashed–dotted horizontal line shows $4\pi\chi' = -0.5$. Inset in panel (c) $\Lambda(h)$ for temperatures between 4.5 and 7.5 K and $H = 85$ Oe. CS regime is identified in h intervals where $\Lambda(h)$ is proportional to ac amplitude (lines are a guide to the eye), and occurs for $h = 1$ Oe above 5.5 K (see text).

Apart from these magnetic mechanisms, pinning by point defects in the superconducting film lead to $N = 1$ [4] and may be related to random pinning by intrinsic defects that have typical sizes smaller than the size of the dots.

Variable h measurements were carried out to identify the CS regime with the purpose of determining the critical current density, $J_C(T)$ [21]. The temperature dependence of J_C is analyzed below and compared to predicted dependences for different pinning interactions [4].

Figures 3(a) and (b) show $\chi''(T, h)$ and $\chi'(T, h)$ respectively, for $h = 0.25$. 0.5, 0.75, 1.0, 1.25, 1.5, 1.75 and 2 Oe, $f = 1$ kHz and applied field $H = 85$ Oe $\approx H_1{}^R$. Arrows indicate increasing ac amplitude. To determine the range of ac amplitude and temperature where the system is in CS, we have followed a procedure described in detail elsewhere [12]. At large enough h vortex displacements become larger than the pinning potential size, the lower h limit depending on temperature and field, and inter-valley motion will dominate over most of the film. In the framework of isotropic Bean CS model [13] in any region of the sample where vortex motion occurs, the persistent current density J_C is uniform. This determines a characteristic Bean penetration length given by the following expression [13],

$$\Lambda(T, h) = \frac{c}{4\pi}\frac{h}{J_C(T)}\,. \qquad (1)$$

In the framework of Bean's model, χ' only depends on Λ/δ, where δ is a characteristic sample dimension. The method consists in identifying data at different T and h that combine to produce the same Λ according to equation (1) [12].

The procedure starts by considering two $\chi'(T)$ curves, one measured for $h^{(1)}$ and the other for $h^{(2)}$ and assuming the

system is in CS, as we show in panel (c) of figure 3. A horizontal (dashed dotted) line is drawn at $\chi'_A = -0.5$ and the line intercepts the curves for $h^{(1)} = 2$ Oe and $h^{(2)} = 1.75$ Oe at points A and B in the figure. As both A and B correspond to the same value χ'_A they must have the same Λ, that is, $\Lambda_A = \Lambda_B$. Next, a vertical line is drawn from B to intersect the curve with $h^{(1)}$ at point C, with its corresponding value χ'_C. As B and C are at the same temperature, and supposing that Bean model is valid, then $J_C(T)$ is the same for both B and C. Following equation (1) for both points, and taking into account that $\Lambda_A = \Lambda_B$:

$$\frac{\Lambda_C}{\Lambda_B} = \frac{h_C}{h_B} = \frac{h^{(1)}}{h^{(2)}}, \tag{2}$$

$$\Lambda_C = \Lambda_A \frac{h^{(1)}}{h^{(2)}}, \tag{3}$$

$$\Lambda_{B,C} = \frac{c}{4\pi} \frac{h_{B,C}}{J_C(T)}. \tag{4}$$

If a new horizontal line is drawn from C in $h^{(1)}$ that intersects D in $h^{(2)}$, again we have $\Lambda_C = \Lambda_D$. Repeating this procedure one arrives to the expression for the penetration depth Λ at E as a function of the penetration depth at A:

$$\Lambda_E = \Lambda_D \frac{h^{(1)}}{h^{(2)}} = \Lambda_A \left(\frac{h^{(1)}}{h^{(2)}}\right)^2;$$
$$\Lambda_G = \Lambda_A \left(\frac{h^{(1)}}{h^{(2)}}\right)^3 = \Lambda_A \gamma^3. \tag{5}$$

Following these calculations one obtains a collection of values for $\chi'_{A,C,E}$ and the resultant $\Lambda_{A,C,E..} = \Lambda_A \gamma^n$ that depend on the arbitrary value for Λ_A, that was arbitrarily chosen as 1. The procedure can be repeated indefinitely, for any pair of curves with different ac amplitudes to arrive to a collection of Λ versus χ' curves. For those amplitudes in which the system is in CS, all curves should collapse into one unique curve and deviations from the universal curve would indicate departures from the Bean CS behavior.

To compare results with the CS model, one can obtain χ' versus h curves for different constant temperatures, and then calculate Λ as a function of h, as shown in the inset in panel (c) of figure 3. In CS regime Λ depends linearly on h at constant T as predicted by equation (1), and the slope (in a linear plot) should be proportional to $1/J_C(T)$. Lines in the inset of panel (c) are a guide to the eye to show the range of linear behavior. We found that for $h = 1$ Oe, Λ has a linear dependence with h in the temperature range above $T \sim 5.5$ K, suggesting that our data above ~5.5 K can be described within the critical model for $h = 1$ Oe.

After obtaining the unique Λ versus χ' curve, for every χ' measured value for $h = 1$ Oe, we determined $\Lambda(T)$ and then we calculated $J_C(T)$ from equation (1), approximating our sample by a thin disk, in which case $4\pi\chi'(\Lambda/\delta) = -0.5$ for $(\Lambda/\delta) = 0.75$, where δ is the sample thickness [22]. In figure 4(a) we plot these results for $H = 85$ Oe $\approx H_1{}^R$ (squares). The same procedure was followed for applied fields $H = 170$ Oe $\approx 2\ H_1{}^R$ (diamonds) and $H = 255$ Oe $\approx 3\ H_1{}^R$ (triangles).

Following the expressions for the different pinning interactions and approximating the superconducting penetration depth, $\lambda \propto (1 - T/T_C)^{-1/2}$ (see [4]) one obtains a temperature dependence for the pinning force $F_P \propto (1 - T/T_C)^N$ and $N = 1$ or $N = 2.5$ for intrinsic pinning or high permeability pinning, respectively.

In order to verify whether the dependence of the penetration depth with temperature can be approximated to $\lambda \propto (1 - T/T_C)^{-1/2}$ in our temperature range, we used the Evtushinsky *et al* [23]. analytical relationship between $\lambda(T)$ and the superconducting gap $\Delta(0)$ as presented by Shapoval and coworkers in [24] with $2\Delta(0)/k_B T_c = 3.53$ [25] and $\lambda(0) = 90$ nm, which is a typical value for Nb thin films [26]. The calculation of $\lambda(T)$ with these parameters for Nb films, leads to a temperature dependence well approximated by $\lambda \propto (1 - T/T_C)^{-1/2}$ in our whole temperature range. Therefore, following the detailed calculations described in 4, we find that the critical current J_C may be approximated to the expression $(1 - t)^N$, with $t = T/T_C$, where the best fit for N identifies the pinning mechanism.

However, $J_C(t)$ in figure 4(a) cannot be satisfactorily fitted in the whole temperature range to the expression $J_C(t) = J_C(0)\ (1 - t)^N$ with $J_C(0)$ and N as fitting parameters, fixing $T_C = T_C{}^R = 7.95$ K. So we fitted the data in the high t range, as shown by the red lines. The obtained exponent for the first matching field is $N = 2.4$ (close to $N = 5/2$) for $t > 0.84 = t_1$. Similar results are obtained for the second and third matching fields with $N = 2.3$ and $N = 2.8$ for $t > 0.80 = t_2$ and $t > 0.77 = t_3$, shown by vertical arrows. The crossover to the low t range is indicated in the figure by the dashed line.

As shown in figure 2, matching effects in $\chi'(t, H)$ for $H_1{}^R$ are not observable in almost the whole examined t range, except above 0.9. For the second matching field, 2 $H_1{}^R$, matching effects in $\chi'(t, H)$ are observed above $t \approx 0.85$. This is close to t_2 where the change in the temperature dependence of J_C occurs. For $H = 3\ H_1{}^R$, the variation in the temperature dependence of J_C is found at $t \approx 0.77$ and the features that appear in $\chi'(t, H)$ discussed above occur for $t > 0.78$. This seems to indicate a correlation between features in vortex mobility and the critical current density having a well established exponent close to 5/2. The absence of matching features at the field dependent low T range may result from the contribution of intrinsic random pinning [4] that has a linear term in $(1 - t)$ and that becomes more significant as the temperature is reduced. This is consistent, in the case of the three magnetic fields, with the absence of matching effects in the field dependent low T range. So, matching effects are detected in the temperature interval where $J_C(t)$ abides by the pinning mechanism which origin is the high magnetic permeability of the magnetic dots. The pinning force per unit volume, $F_P(t) = J_C(t) \times B$, is plotted in figure 4(b). We assume that F_P is isotropic and that $B = H$, as the sample is fully penetrated by the dc field.

As mentioned above, t_1 and t_2 indicated by arrows in figure 4, show the crossover temperatures above which

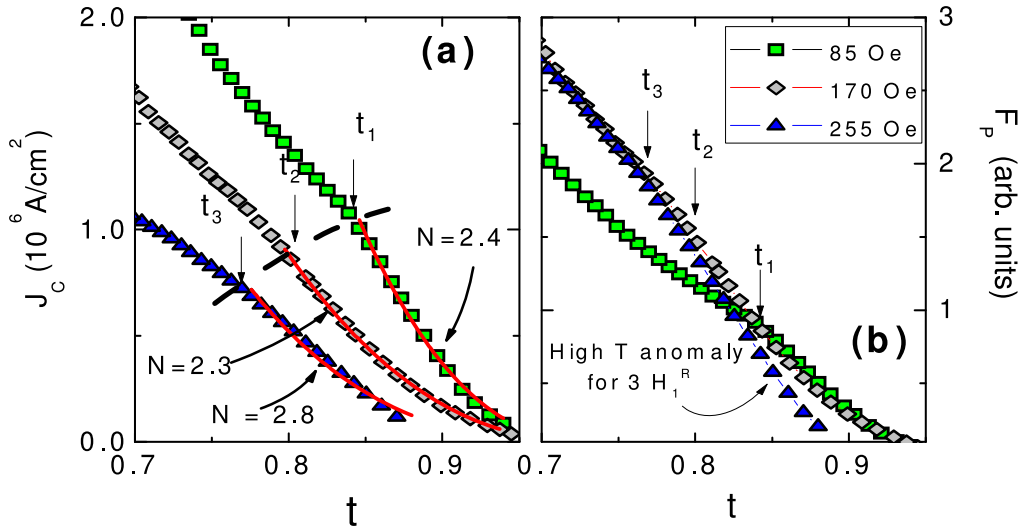

Figure 4. (a) Critical current density, $J_C(T)$, for applied fields $H = 85$ Oe $\approx H_1^R$ (green squares), $H = 170$ Oe $\approx 2\ H_1^R$ (gray diamonds) and $H = 255$ Oe $\approx 3\ H_1^R$ (blue triangles). Red lines are a fit to the expression $J_C = J_C(0)\ (1 - T/T_C)^N$ with $T_C = 7.95$ K (see text). The fitted exponent, $N \sim 5/2$, is indicated for the high t range for each applied field. The dashed line is a guide to show the change in regime, at temperatures t_1, t_2 and t_3 indicated by arrows. (b) $F_P = J_C \times B$ as a function of t where t_1, t_2 and t_3 are again indicated by arrows (see text).

magnetic pinning dominates for H_1^R and $2\ H_1^R$ respectively, and $F_P(t)$ coincides for the first and the second matching fields in this pinning regime. This implies that the additional interstitial vortex line in every pinning cell for $H = 2H_1^R$ does not modify the pinning strength when the vortex interaction with the high permeability of Ni dots dominates the pinning mechanisms, although additional vortex lines make the VL stiffer and extend the high t pinning range. However, in the low temperature range where intrinsic pinning dominates, $F_P(t)$ is lower when no interstitial vortices are present for $H = H_1^R$, implying that the additional interstitial vortex does contribute to the pinning force.

On the other hand, below t_3, the pinning force for $H = 2H_1^R$ is equal to the pinning force for $H = 3H_1^R$, suggesting that a second interstitial vortex line does not modify the low temperature force. The anomalous low pinning force for $H = 3H_1^R$ at temperatures above $t_3 = 0.77$, is in coincidence with the local maxima in χ' $(3H_1^R)$, and is probably related to the competition between rectangular and square VL arrays, resulting the high t exponent $N = 2.8$ for the critical current (see figure 4(a)).

4. Summary and conclusions

We have used ac susceptibility techniques, χ_{ac}, to study the dynamics of the VL in Nb films containing two-fold rectangular arrays of Ni dots well below T_C.

We found that matching periodicity, at integer multiples of the first rectangular matching field H_1^R is tainted, and it is originated in vortex motion driven by azimuthally induced currents, alternatively parallel to the long and short side of the rectangular array in different parts of the sample simultaneously.

Instead of observing a reconfiguration transition as field is increased, from rectangular to square matching periodicity reported in dc transport experiments, we observe that for applied fields that are simultaneously multiples of H_1^R and of the first matching field, H_1^S, for a square of sides equal to the short side of the rectangular pinning array, mobility increases. The coincidence occurs due to the aspect ratio, $a_R = 3/2$ of the rectangular array, and we conclude that competing VL configurations at these 'matching' orders lead to an overall anomalous decrease in pinning.

We identified the Bean critical state (CS) regime with a known procedure, and we extracted $J_C(T,H)$ from our $\chi_{ac}(T, H)$ data. The VL pinning mechanism was examined by studying the temperature dependence of $J_C(T)$ at the first three matching fields.

By comparing the temperature dependence of the experimental pinning forces with theoretical models, we were able to identify the prevailing pinning interaction. Above a crossover temperature dependent on the stiffness of the vortex array, pinning arises from the interaction between the vortex lines and the high permeability of ferromagnetic dots. Consistently, there is a correlation between matching features in vortex mobility and the critical current density having the predicted well established exponent close to 5/2 that corresponds to this interaction.

Interestingly, in this regime, the presence of an extra interstitial vortex line for $2\ H_1^R$ does not modify the effective pinning force, but it clearly increases pinning in the low temperature regime where intrinsic pinning comes into play, making no difference whether one or two additional interstitial vortices are present.

Acknowledgments

We acknowledge the support from Argentina FONCyT grant PICT 2008 N° 753 and UBA grant UBACyT N° 661. We also thank the support from Spanish MINECO grants

FIS2008-06249 (Grupo Consolidado), FIS2013-45469 and EU Cost Action MP-1201.

References

[1] Vélez M, Martín J I, Villegas J E, Hoffmann A, González E M, Vicent J L and Schuller Ivan K 2008 *J. Magn. Magn. Mater.* **320** 2547 and references therein

[2] Martín J I, Vélez M, Nogués J and Schuller Ivan K 1997 *Phys. Rev. Lett.* **79** 1929

[3] Van Bael M J, Temst K, Moshchalkov V V and Bruynseraede Y 1999 *Phys. Rev.* B **59** 14674

[4] Martín J I, Vélez M, Hoffmann A, Schuller Ivan K and Vicent J L 2000 *Phys. Rev.* B **62** 9110

[5] Jaccard Y, Martín J I, Cyrille M-C, Vélez M, Vicent J L and Schuller Ivan K 1998 *Phys. Rev.* B **58** 8232

[6] Morgan David J and Ketterson J B 1998 *Phys. Rev. Lett.* **80** 3614

[7] Metlushko V *et al* 1999 *Phys. Rev.* B **60** R12585

[8] Villegas J E, Gonzalez E M, Montero M I, Schuller Ivan K and Vicent J L 2003 *Phys. Rev.* B **68** 224504

[9] Martín José I, Vélez M, Hoffmann A, Schuller Ivan K and Vicent J L 1999 *Phys. Rev. Lett.* **83** 1022

[10] Stoll O M, Montero M I, Guimpel J, Akerman Johan J and Schuller Ivan K 2002 *Phys. Rev.* B **65** 104518

[11] Chiliotte C E, Carreira S J, Bekeris V, Gomez A, Gonzalez E M, Prieto J L and Vicent J L 2013 *IEEE Trans. Magn.* **49** 4643

[12] Pasquini G, Civale L, Lanza H and Nieva G 1999 *Phys. Rev.* B **59** 9627

[13] Bean C P 1962 *Phys. Rev. Lett.* **8** 250

[14] Hoffmann A, Prieto P and Schuller Ivan K 2000 *Phys. Rev.* B **61** 6958

[15] Martín J I, Jaccard Y, Hoffmann A, Nogués J, George J M, Vicent J L and Schuller Ivan K 1998 *J. Appl. Phys.* **84** 411

[16] See for example Civale L, Worthington T K, Krusin-Elbaum L and Holtzberg F 1992 *Magnetic Susceptibility of Superconductors and Other Spin Systems* ed R A Hein, T L Francavilla and D H Liebenberg (New York: Plenum) p 313

[17] Mkrtchyan G S and Shmidt V V 1972 *Sov. Phys. JETP* **34** 195 Buzdin A and Feinberg D 1996 *Physica* C **256** 303 Nordborg H and Vinokur V M 2000 *Phys. Rev.* B **62** 12408

[18] Gomez A, del Valle J, Gonzalez E M, Chiliotte C E, Carreira S J, Bekeris V, Prieto J L, Schuller Ivan K and Vicent J L 2014 *Supercond. Sci. Technol.* **27** 065017

[19] Reichhardt C, Zimányi G T and Grønbech–Jensen Niels 2001 *Phys. Rev.* B **64** 014501

[20] Vélez M, Jaque D, Martín J I, Guinea F and Vicent J L 2002 *Phys. Rev.* B **65** 094509

[21] Dew-Hughes D 1974 *Phil. Mag.* **30** 293

[22] Clem John R and Alvaro Sanchez 1994 *Phys. Rev.* B **50** 9355

[23] Evtushinsky D V *et al* 2009 *New J. Phys.* **11** 055069

[24] Shapoval T, Stopfel H, Haindl S, Engelmann J, Inosov D S, Holzapfel B, Neu V and Schultz L 2011 *Phys. Rev.* B **83** 214517

[25] Antonova E A, Dzhuraev D R, Motulevich G P and Sukhov V A 1981 *Sov. Phys. JETP* **53** 1270

[26] Zhang Huai Lynn J W, Majkrzak C F, Satija S K, Kang J H and Wu X D 1995 *Phys. Rev.* B **52** 10395